

INFORMATION NOT TO BE
RELEASED OUTSIDE NASA
UNTIL PAGE PRESENTED

UNSTEADY LIFT FORCES GENERATED BY VORTEX SHEDDING ABOUT
A LARGE, STATIONARY, AND OSCILLATING CYLINDER AT
HIGH REYNOLDS NUMBERS

By George W. Jones, Jr.

NASA Langley Research Center
Langley Station, Hampton, Va.

Presented at the ASME Symposium on Unsteady Flow
(Fluids Engineering Division)

N 68-34326	
(ACCESSION NUMBER)	(THRU)
<u>31</u> (PAGES)	<u>1</u> (CODE)
<u>TMX 601214</u> (NASA CR OR TMX OR AD NUMBER)	<u>12</u> (CATEGORY)

Philadelphia, Pennsylvania
May 6-9, 1968

GPO PRICE \$ _____

CSFTI PRICE(S) \$ _____

Hard copy (HC) 3.00

Microfiche (MF) 1.65

UNSTEADY LIFT FORCES GENERATED BY VORTEX SHEDDING ABOUT
A LARGE, STATIONARY, AND OSCILLATING CYLINDER AT
HIGH REYNOLDS NUMBERS

By George W. Jones, Jr.

NASA Langley Research Center

ABSTRACT

A wind-tunnel study has been made of the unsteady lift (crosswind) forces on a large, two-dimensional cylinder with axis perpendicular to the flow. The forces were measured at Reynolds numbers from 0.36 million to 18.7 million at Mach numbers up to 0.6 with the cylinder held both stationary and oscillated laterally. The mean-drag and the Strouhal number of the unsteady lift forces on the stationary cylinder followed the trends established by previous investigators. At higher, hitherto unexplored Reynolds numbers, the mean-drag was approximately 0.54, and the Strouhal number was approximately 0.3. The unsteady root-mean-square lift force on the stationary cylinder was defined over the flow parameter range investigated. For the oscillated cylinder, an unsteady lift force due to motion was found to exist at cylinder frequencies near the vortex-shedding frequency of the stationary cylinder. This unsteady lift due to motion was found to be a destabilizing aerodynamic damping force at frequencies below the stationary cylinder vortex-shedding frequency which shifted abruptly to a stabilizing damping force at frequencies above the vortex-shedding frequency.

INTRODUCTION

Recently, the response to ground winds of large flexible structures such as metal smokestacks and cylindrical space vehicles standing on the launch pad has led to considerable interest in the spontaneously generated unsteady aerodynamic forces on circular cylinders at high Reynolds numbers. These unsteady forces are produced by vortices shed alternately from the sides of the structure and, for lightly damped structures, are capable of exciting large amplitude vibratory response. The unsteady forces associated with vortex shedding are not well understood or amenable to analysis. Many investigators have made experimental studies such as given in references 1 to 11 which have given some understanding of the mechanism of vortex shedding, particularly at lower Reynolds numbers. However, at higher Reynolds numbers, there is little information on the nature of these aerodynamic forces. In particular, the question of how these forces are affected by the motion of the structure as it deflects in response to the aerodynamic loads has needed investigation.

A wind-tunnel investigation has, therefore, been conducted on a large circular cylinder in a two-dimensional flow at Reynolds numbers from 0.36 million to 18.7 million. The cylinder was instrumented to read directly the mean-drag and unsteady lift forces. In addition to being fixed, the cylinder could be oscillated over a range of frequencies and amplitudes. This oscillation capability was used to investigate the effects of cylinder motion on the aerodynamic forces generated. Figure 1 presents a comparison of the Reynolds number and nondimensional frequency-of-oscillation ranges of the present investigation with those of previous investigations. This figure shows the present

investigation has greatly extended the range of Reynolds number and nondimensional frequency of oscillation over which the aerodynamic forces on cylinders have been studied.

The investigation was a joint effort by NASA, Marshall Space Flight Center, and NASA, Langley Research Center, together with The Martin Company, Baltimore. The Martin Company, under contract, supplied the model and participated in the tests and some data reduction. Results of this investigation, based on preliminary data reduction, were given in reference 12. The present paper will first briefly review some of the major results obtained in the study and show some comparison with other investigators which was lacking in reference 12. Then the paper will concentrate on the effects of cylinder motion on the unsteady lift forces. It should be pointed out that the data on cylinder-motion effects presented in reference 12 indicated correct trends, but were quantitatively in error.

SYMBOLS

A	projected area of instrumented section of cylinder
C_D	mean-drag coefficient for instrumented section of cylinder
$C_{L,Imag}$	imaginary component (in phase with cylinder velocity) of the aerodynamic-lift-coefficient vector at the frequency of oscillation of the cylinder
$C_{L,Re}$	real component (in phase with cylinder displacement) of the aerodynamic-lift-coefficient vector at the frequency of oscillation of the cylinder
$C_{L,rms}$	root-mean-square value of unsteady-lift coefficient on instrumented section of cylinder
$C_{p,base}$	average of section-pressure coefficients at rear of cylinder between $\phi = 150^\circ$ and $\phi = 210^\circ$
D	diameter of test cylinder, 3 feet (0.9144 meter)

f	frequency, Hz
f_h	forcing frequency of cylinder oscillation, Hz
f_s	vortex-shedding frequency, Hz
h	instantaneous amplitude of cylinder displacement under forced oscillation, $h = h_0 \cos \omega t$
h_a	Scruton-type aerodynamic derivative of real component of unsteady-lift-force-coefficient vector at frequency of cylinder oscillation, $\frac{-C_{L,Re}}{2S^2\left(\frac{h}{D}\right)}$
h_0	amplitude (0-peak) of cylinder displacement
k_a	Scruton-type aerodynamic derivative of imaginary component of unsteady-lift-force-coefficient vector at frequency of cylinder oscillation, $\frac{-C_{L,Imag}}{4\pi S^2\left(\frac{h}{D}\right)}$
M	Mach number
q	free-stream dynamic pressure, $\frac{1}{2} \rho V^2$
R_N	Reynolds number based on cylinder cross-section diameter
S	aerodynamic Strouhal number, $\frac{f_s D}{V}$
t	time
V	velocity of test medium
ζ	viscous damping ratio
ρ	density of test medium
φ	angular location of static pressure orifice with respect to direction of free-stream flow
$\Phi_{C_L}(S)$	power spectral density of unsteady-lift-force coefficient as function of Strouhal number, $(Lift)^2 = (qA)^2 \int_0^\infty \Phi_{C_L}(S) dS$
ω	circular frequency

APPARATUS AND TESTS

The Langley transonic dynamics wind tunnel used for the investigation has a test section approximately 16 feet (4.877 meters) square with cropped corners and the unique ability to use either air or Freon 12 as a test medium. A photograph of the cylinder model mounted in the tunnel is shown in figure 2. Although the model cross-section area appears large in relation to the tunnel cross-section area, the estimated solid-blockage interference was negligible, and no wall-interference corrections have been made to the data.

The cylinder model has a 3-foot (0.914-meter) diameter and spanned the tunnel with its longitudinal axis perpendicular to the air flow. The model structure consisted of an inner support cylinder, an outer cylinder divided into sections, a variable-stiffness suspension system, and a hydraulic shaker system. The inner cylinder, a seamless aluminum tube, carried the load and extended through the tunnel floor and ceiling to attach to the suspension system. The outer-cylinder sections were of lightweight aluminum honeycomb sandwiched between thin aluminum sheets. The top and bottom outer-cylinder sections were rigidly fastened to the inner cylinder with spacers. A 7-foot (2.1336-meter) center section of the outer cylinder was attached to the inner cylinder by force transducers, oriented so as to read directly the integrated forces on the center section in the direction of and at right angles to the flow. The 0.02-inch (0.0408-cm) gaps between the fixed top and bottom sections of the outer cylinder and the instrumented center section were originally designed with a labyrinth seal which proved unsatisfactory, and was supplemented by filling the gaps with a silicone rubber compound. This flexible rubber seal allowed relative motion between adjacent cylinder sections and

transmitted in shear only about 1 percent of the load on the center section. The suspension system consisted of one tapered torque bar attached to the top of the cylinder and an identical bar attached to the bottom of the cylinder. Remotely controlled clamping mechanisms could be positioned along the torque bars so as to change the resonant frequency of the system over a range from 3 to 20 Hz. Two hydraulic shakers, one positioned at the top and the other at the bottom of the cylinder, were driven from a single control, and could either hold the cylinder fixed or impart an oscillatory driving force at right angles to the tunnel flow on the resonant system over the range of resonant frequencies at amplitudes up to 3 inches displacement.

A Martin-developed instrumentation system called the Inertia Compensated Balance was used to measure directly the aerodynamic forces on the 7-foot (2.1336-meter) outer-cylinder section in the plane of the flow and at right angles to the flow. This ICB system electrically combined the signals from the strain-gage force transducers with the signals from two strategically located accelerometers in such a manner as to cancel out the forces due to inertia and thus give a direct measure of the aerodynamic forces. A single row of static-pressure orifices measured the static-pressure distribution around the cylinder at one longitudinal station, 1.14 diameters from the lower end of the model.

During the test program, the mean-drag and unsteady lift forces were measured at Reynolds numbers from 0.36 to 18.7 million at Mach numbers up to 0.6 with the cylinder held fixed and with the cylinder oscillated at model reduced frequency, $\frac{f_h D}{V}$, from 0.06 to 0.50. Static pressures were measured only with the cylinder held fixed.

SELECTED RESULTS AND DISCUSSION

As stated in the introduction, the results presented here will briefly review some of the mean-drag and unsteady lift data covered in reference 12, giving comparisons with other data not presented in reference 12. Following this review, the results for the aerodynamic forces on the moving cylinder will be presented since these results, as presented in reference 12, are incomplete and quantitatively in error.

Mean-Drag Data

The mean-drag data measured on the cylinder at $M \leq 0.2$ are presented in figure 3 and compared with data from previous investigators. These data are particularly meaningful for ground winds on launch vehicles or similar large cylindrical structures where Mach numbers are low but Reynolds numbers are high. The trends from four different sources agree well; however, at given Reynolds numbers the differences in measured drag coefficients are appreciable. The greater drag on Roshko's sandblasted pipe cylinder, as compared with the drag on the smooth cylinder of this investigation, was probably caused by the difference in roughness of the two cylinders. The data show that, for a smooth cylinder, the drag coefficient increases from 0.15 at $R_N \approx 0.5 \times 10^6$ to about 0.54 at $R_N \approx 3 \times 10^6$, and then decreases slightly as Reynolds number increases to 10×10^6 .

The variation of base pressure coefficient is presented in figure 4 for Mach number ≤ 0.2 . Base pressure data from references 5 and 8 are also presented for comparison. Note that these base pressures show the same trends as the drag coefficients of figure 3.

Characteristics of Unsteady Lift Measured on Stationary Cylinder

Frequency content of unsteady lift.- The unsteady lift on a stationary cylinder can be periodic, random, or combinations of both forms. In order to deal with these forms, a classification of the unsteady lift on a stationary cylinder in terms of the frequency content has been adopted as follows:

The usual nondimensional aerodynamic Strouhal number is defined as $S = \frac{f_s D}{V}$ where f_s is the vortex-shedding frequency of the cylinder. If a power spectral density plot is made from a time history data sample of the unsteady lift force, and the frequency of the main peak in this plot is defined to be f_s , then the frequency interval between the half-power points of this spectrum peak may be defined as the Strouhal bandwidth. Figure 5 shows, in inset form, a typical power spectral density plot with the Strouhal bandwidth indicated. The larger plot shows the variation of this Strouhal bandwidth with Reynolds number. These data are limited to $M < 0.3$. From study of this plot and the associated autocorrelation and probability-density functions determined from the data time history samples, the frequency content of the unsteady lift on the stationary cylinder may conveniently be divided into the three regimes indicated in figure 5. These regimes and the Reynolds number ranges over which they apply are wide-band random ($1.1 \times 10^6 < R_N < 3.5 \times 10^6$), narrow-band random ($3.5 \times 10^6 < R_N < 6.0 \times 10^6$), and quasi-periodic ($R_N > 6.0 \times 10^6$). The wide-band random forces occur in what has been termed the "supercritical" Reynolds number range in references 2, 5, and 8. The quasi-periodic forces occur in the "transcritical" Reynolds number range of reference 5, and the narrow-band random forces occur in an intermediate or transition range between the wide-band random and quasi-periodic regimes.

Previous investigators have presented the frequency characteristics of the unsteady lift force in terms of a single aerodynamic Strouhal number rather than a Strouhal bandwidth. For purposes of comparison, the data of the present investigation are presented in this form in figure 6. Also presented for comparison are data from other investigators. The shaded areas denote ranges where a definite, easily defined vortex-shedding frequency occurred. In the Reynolds number range from about 0.56 million to 2.6 million, there is no distinct frequency, and all investigators had difficulty in identifying a predominant frequency. This fact may account for the considerable scatter in this region. It is seen that there is good agreement between the present data and that of Roshko (ref. 5) in the Reynolds number range between 3.7 million and 8.4 million, and that in the previously unexplored region between 8.4 million and 18 million the Strouhal number remains relatively constant at about 0.3.

Magnitude of unsteady lift.- The root-mean-square lift coefficients on the stationary cylinder at $M \leq 0.3$ and $M = 0.4$ are presented in figure 7 as functions of Reynolds number. Also presented for comparison are similar data from Fung (ref. 2) and Schmidt (refs. 7 and 8). Examination of this figure shows that for the data at $M \leq 0.3$, the unsteady lift appears to be multiple valued at Reynolds numbers below about 8 million. This phenomenon is believed to be related to roughness asymmetries in the laminar flow regions on the cylinder. These asymmetries change from time to time as small particles, or scratches collect on the upstream surface of the cylinder during a test, and therefore give rise to apparent scatter in the data. Above 8 million Reynolds number, where the flow is turbulent, the root-mean-square lift coefficient measurements were repeatable and followed the single curve shown in figure 7. Thus, the multiple-valued data seem to occur at Reynolds numbers corresponding

to those for the wide-band and narrow-band ranges of Strouhal numbers and merge to a single-valued boundary at Reynolds number where the vortex shedding is quasi-periodic. For Mach number 0.4, the lift coefficient measurements are repeatable for all points shown in figure 1, and there is a large Mach number effect at Reynolds numbers from 7 million to 17 million as shown by the rounded peak in the data at a Reynolds number of about 9 million.

Comparative data from Fung (ref. 2) and Schmidt (refs. 7 and 8) are shown in figure 7 in the form of broad bands because of scatter in the individual data points. Both sets of comparative data tend to merge into the data of the present investigation. Fung's data (ref. 2) approach the upper part of the multiple-valued region, and Schmidt's data (refs. 7 and 8) merge with the lower part of this region. Thus, the unsteady lift coefficients obtained on the stationary cylinder are consistent with the trends of previous data.

Characteristics of Unsteady Lift Due to Cylinder Motion

In order to investigate the effects of cylinder motion on the unsteady lift force, a positive displacement sinusoidal oscillation was imparted to the model by the hydraulic shakers at the top and bottom of the cylinder. The model was driven at frequencies from 3 to 18.7 Hz and amplitudes to 3 inches (0.0762 meter). The forces in the lift direction were measured on the 7-foot (2.1336-meter) center cylinder section using the Inertia Compensated Balance system, and the data thus obtained were reduced using a variety of techniques. The major results will be presented first in terms of the same characteristics used to describe the lift on the stationary cylinder. Next, by playing the tape recorded data samples of unsteady lift force into a special purpose analog computer, the in-phase and 90° out-of-phase (real and imaginary) components of

the unsteady lift force with respect to displacement were determined at the frequency of motion. Results from this analysis are then presented.

Power spectral density and root-mean-square values.- Figure 8 presents the power spectral density of the lift force in coefficient form for two data points at the same Mach number and Reynolds number. For one data sample the cylinder was held stationary, and for the other the cylinder was oscillated at the aerodynamic Strouhal frequency of the stationary cylinder ($S = 0.31$). A large increase in the peak of the spectrum for the moving cylinder is readily apparent. The root-mean-square lift coefficient increased from 0.0762 to 0.1296. Thus, this comparison shows the existence of a lift due to motion.

In order to show the ratio of this unsteady lift due to motion to the unsteady lift on the stationary cylinder, selected values of the root-mean-square coefficient of lift on the moving cylinder were normalized by corresponding values on the stationary cylinder. The results are plotted in figure 9 as functions of nondimensional frequency ratio and cylinder amplitude of motion. The frequency ratio is the nondimensional frequency of forced oscillation, $\frac{f_n D}{V}$, divided by the aerodynamic Strouhal number for the stationary cylinder. The data for this figure have been restricted to Mach numbers less than 0.3 and Reynolds numbers greater than 5.5×10^6 , where Mach number effects are small and the periodicity of the flow is clearly defined.

The lift coefficient ratios of figure 9 show that when the cylinder is oscillated in the lift plane at frequencies far removed from the aerodynamic Strouhal frequency, there is no increase, or, in some cases, a slight decrease in lift over that of the stationary cylinder. However, for cylinder motion at or near the Strouhal frequency, there is a definite lift due to motion, and this lift increases with amplitude of cylinder motion. The maximum

amplification of the lift due to motion occurs when the frequency is approximately equal to 0.99 and increases with increasing amplitude as indicated by the small plot at the lower right-hand side of figure 9.

Lift force vector at frequency of cylinder oscillation.- Examination of data such as shown in figures 8 and 9 and of the time histories of the lift force on the oscillating cylinder indicated a likelihood of correlation between the aerodynamic forces and the cylinder motion. Therefore, an analysis was made using the tape recorded time histories of the unsteady lift force from the data samples of figure 9 and the corresponding time histories of sinusoidal cylinder motion. This analysis determined the aerodynamic force components that are in phase (real component) and 90° out of phase (imaginary component) with the sinusoidal displacement. The results of this analysis are presented in figure 10 which gives the real and imaginary vector components with respect to the displacement of the lift force on the moving cylinder at the frequency of cylinder oscillation. These components have been normalized by the root-mean-square lift component on the stationary cylinder and are presented as functions of nondimensional frequency ratio and amplitude.

The real component may be thought of as an aerodynamic stiffness parameter, and it behaves much as the root-mean-square unsteady lift on the oscillating cylinder (fig. 9) in that the real component (fig. 10(a)) of the lift vector is substantial only when the cylinder oscillates at or near the aerodynamic Strouhal frequency, and this component increases with increasing cylinder amplitude of motion. It should be noted that the apparent mass effects are not included in this real component since the Inertia Compensated Balance system cancels them out even though they might legitimately be included here.

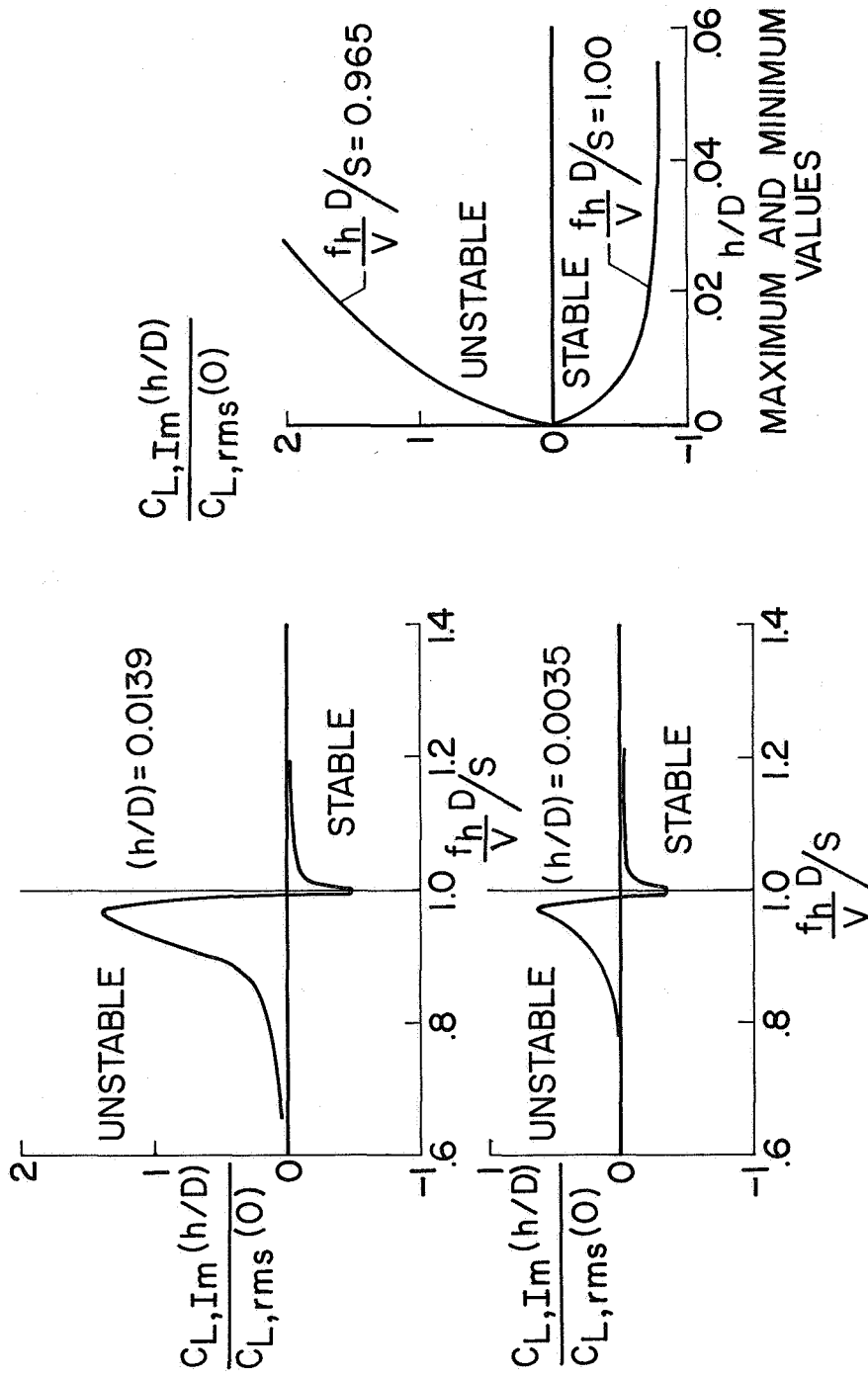


Figure 10b.- Damping component of unsteady lift due to cylinder motion.

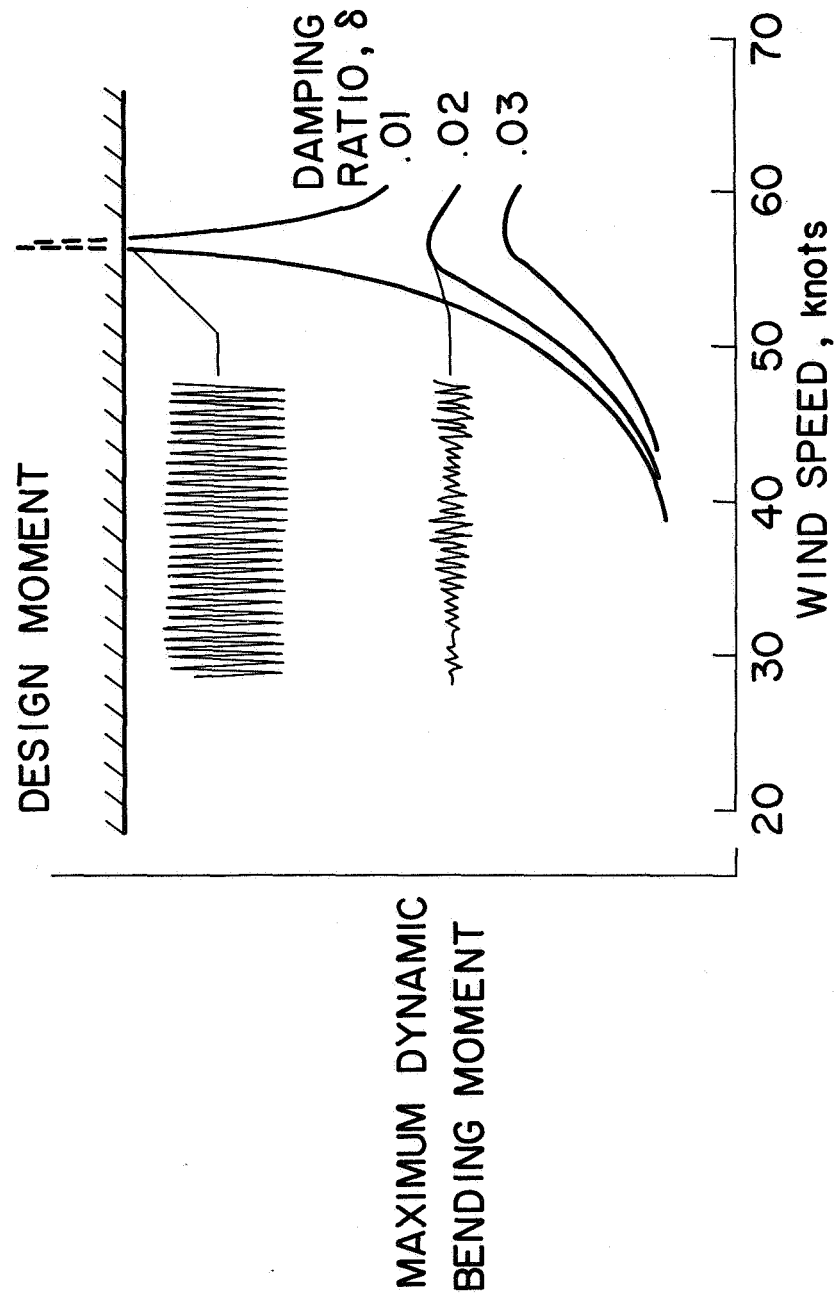


Figure 11.- Effect of damping on Saturn V ground wind loads.

Similarly, the imaginary component of the lift coefficient vector (fig. 10(b)), being in phase with the velocity, may be regarded as an aerodynamic damping parameter. This component of the unsteady lift due to motion was found to be a destabilizing aerodynamic damping force at frequencies below the stationary cylinder vortex-shedding frequency. This force shifts abruptly to a stabilizing damping force at frequencies above the vortex-shedding frequency. Also, this damping component changes with amplitude of motion as shown in the small inset figure at the lower right.

These real and imaginary lift coefficients can be converted into aerodynamic derivatives such as used by Scruton in reference 4. The relationships between Scruton's derivatives and the real and imaginary lift coefficients of figure 10 are

$$-h_a = \frac{C_{L,Re}}{2S^2 \left(\frac{h}{D}\right)} \quad \text{and} \quad -k_a = \frac{C_{L,Imag}}{4\pi S^2 \left(\frac{h}{D}\right)}$$

For flexible structures such as a launch vehicle on its pad, a nonlinear aerodynamic damping term such as $-k_a$ can give rise to a self-excited limit amplitude sinusoidal oscillation. Such oscillations have been observed on aeroelastic ground wind load models of launch vehicles (ref. 13) and on other structures (ref. 14).

Figure 11 shows a typical example of such an oscillation on a Saturn V aeroelastic ground wind loads model where the maximum dynamic bending moment at the base of the vehicle on the launch pad is plotted against wind speed in knots. At wind speed of about 57 knots, which corresponds to a Strouhal number of about 0.2 based on the diameter of the lower stages, the response peaks sharply. At a low value of structural damping, $\zeta = 0.01$, the time

history of response is nearly sinusoidal. This feature implies the existence of a self-excited limit-amplitude oscillation for which the negative aerodynamic-damping term and positive structural-damping term are in equilibrium. At higher values of structural damping, such as $\zeta = 0.02$, the response time history changes to a random-amplitude constant-frequency motion which is typical of the response of a lightly damped mechanical system to a random forcing function.

CONCLUSIONS

Analysis of the results presented from a wind-tunnel study of the mean-drag and unsteady lift forces on a stationary and oscillating circular cylinder in two-dimensional flow at Reynolds numbers from 0.36 million to 18.7 million indicates the following conclusions:

1. The mean-drag coefficient on the stationary cylinder, at Mach numbers less than about 0.2, follows the trends established by previous investigators and has an approximately constant value of 0.54 for Reynolds numbers between 4 million and 10 million.

2. The frequency content of the unsteady lift force on the stationary cylinder can be categorized into three regimes dependent upon Reynolds number as follows: wide-band random ($1.4 \times 10^6 < R_N < 3.5 \times 10^6$), narrow-band random ($3.5 \times 10^6 < R_N < 6.0 \times 10^6$), and quasi-periodic ($R_N > 6.0 \times 10^6$).

3. The Strouhal number of the unsteady lift on the stationary cylinder in terms of the center frequency of a Strouhal bandwidth follows the trends established by previous investigators at Reynolds numbers from 1.4 million to 8 million, then at hitherto unexplored Reynolds numbers from 8 million to 17 million is approximately constant at about 0.3.

4. At Mach numbers less than 0.3, the root-mean-square unsteady lift coefficient on the stationary cylinder fluctuates at Reynolds numbers from 1.5 million to 8 million, then the range narrows into a single function which decreases slowly with higher Reynolds numbers.

5. A lift force due to cylinder oscillation exists when the cylinder is oscillated at or near the aerodynamic Strouhal frequency of the stationary cylinder. This lift force increases with increase in amplitude of motion, building up to several times the lift on the stationary cylinder. When the cylinder is oscillated at frequencies far removed from the aerodynamic Strouhal frequency of the stationary cylinder, there is no significant lift due to motion.

6. The unsteady lift due to motion was found to have a destabilizing aerodynamic damping component for cylinder motion at frequencies below the stationary cylinder vortex-shedding frequency. This component shifts abruptly to a stabilizing damping force at frequencies above the vortex-shedding frequency.

REFERENCES

1. Relf, E. F.; and Simmons, L. F. G.: The Frequency of Eddies Generated by Motion of Circular Cylinders Through a Fluid. R. & M. 917, British A.R.C., 1924.
2. Fung, Y. D.: Fluctuating Lift and Drag Acting on a Cylinder in a Flow at Supercritical Reynolds Numbers. Jour. Aerospace Sci., vol. 27, no. 11, November 1960, pp. 801-804.
3. Humphreys, J. S.: On a Circular Cylinder in a Steady Wind at Transition Reynolds Numbers. Jour. of Fluid Mechanics, vol. 9, part 4, December 1960, pp. 603-612.
4. Scruton, C.: On the Wind Excited Oscillations of Stacks, Towers, and Masts. National Physical Laboratory, paper 16, June 1963.
5. Roshko, Anatol: Experiments on the Flow Past a Circular Cylinder at Very High Reynolds Number. Jour. of Fluid Mechanics, vol. 10, part 3, May 1961, pp. 345-356.
6. Flachsbart, O.: 1929. From an article by H. Muttray 1932, Handb. Experimental Physik, 4, part 2 (Leipzig), p. 316.
7. Schmidt, L. V.: Measurements of Fluctuating Air Loads on a Circular Cylinder. Jour. of Aircraft, vol. 2, no. 1, 1965, pp. 49-55.
8. Schmidt, L. V.: Fluctuating Force Measurements Upon a Circular Cylinder at Reynolds Number Up to 5×10^6 . From paper presented at meeting on Ground Wind Loads Problems in Relation to Launch Vehicles. NASA TM X-57779, 1966, pp. 19.1-19.17.
9. Goldman, R. L.: Karman Vortex Forces on the Vanguard Rocket. Shock and Vibration Bulletin, Part II, U.S. Naval Research Lab., Washington, D.C., December 1958.
10. Delany, Noel K.; and Sorensen, Norman E.: Low-Speed Drag of Cylinders of Various Shapes. NACA TN 3038, November 1953.
11. Bishop, R. E. D.; and Hassan, A. V.: The Lift and Drag Forces on a Circular Cylinder Oscillating in a Flowing Fluid. Proc. Roy. Soc. A, 277, 1964, pp. 51-75.
12. Cincotta, J. J.; Jones, G. W., Jr.; and Walker, R. W.: Experimental Investigation of Wind Induced Oscillation Effects on Cylinders in Two-Dimensional Flow at High Reynolds Numbers. NASA TM X-57779, 1966, pp. 20.1-20.35.

13. Reed, Wilmer H., III: Models for Obtaining Effects of Ground Winds on Space Vehicles Erected on the Launch Pad. Conference on the Role of Simulation in Space Technology, Virginia Polytechnic Institute, Engineering Extension Series, Circular No. 4, Part C, August 17-21, 1964.

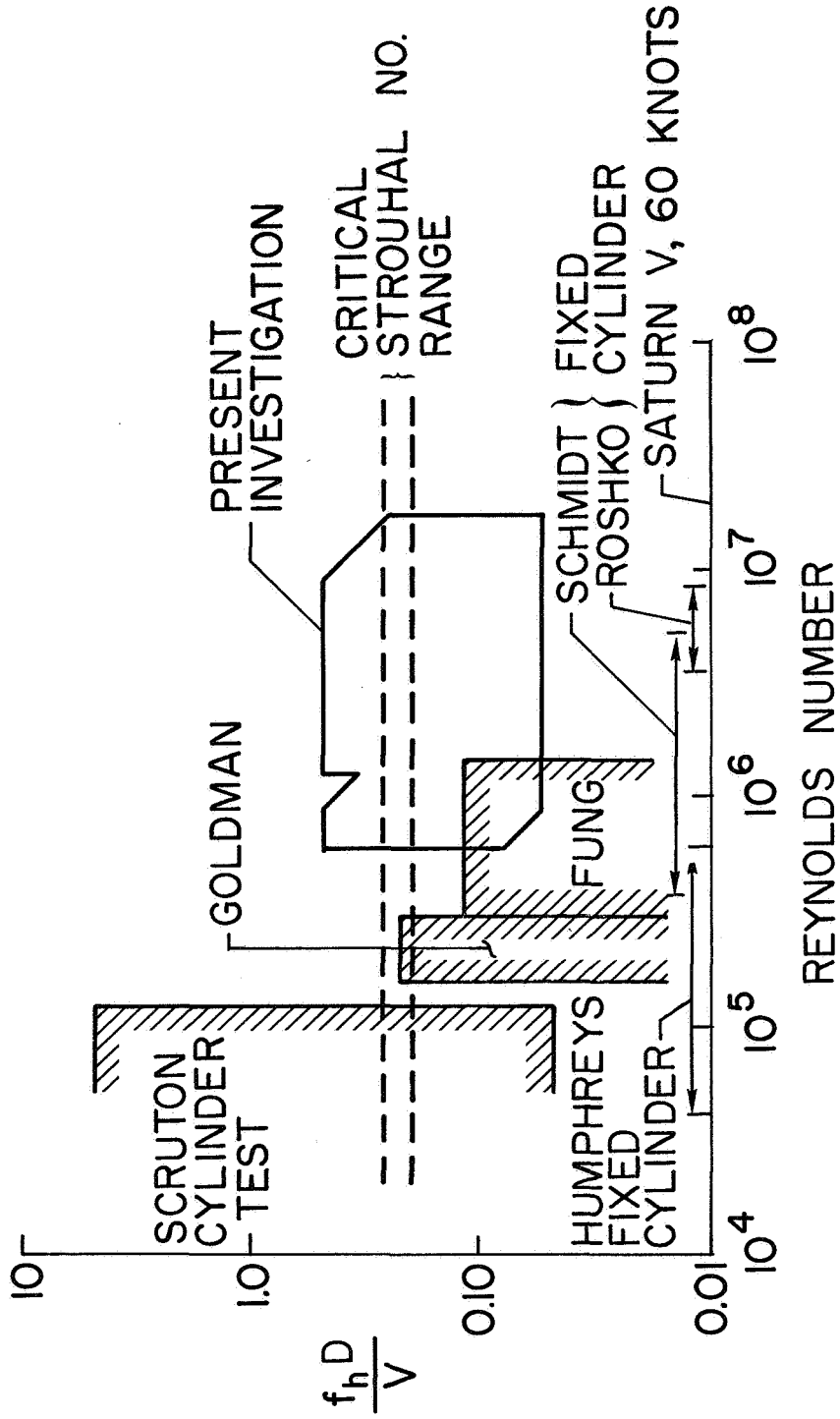


Figure 1.- Comparison of present and previous investigations.

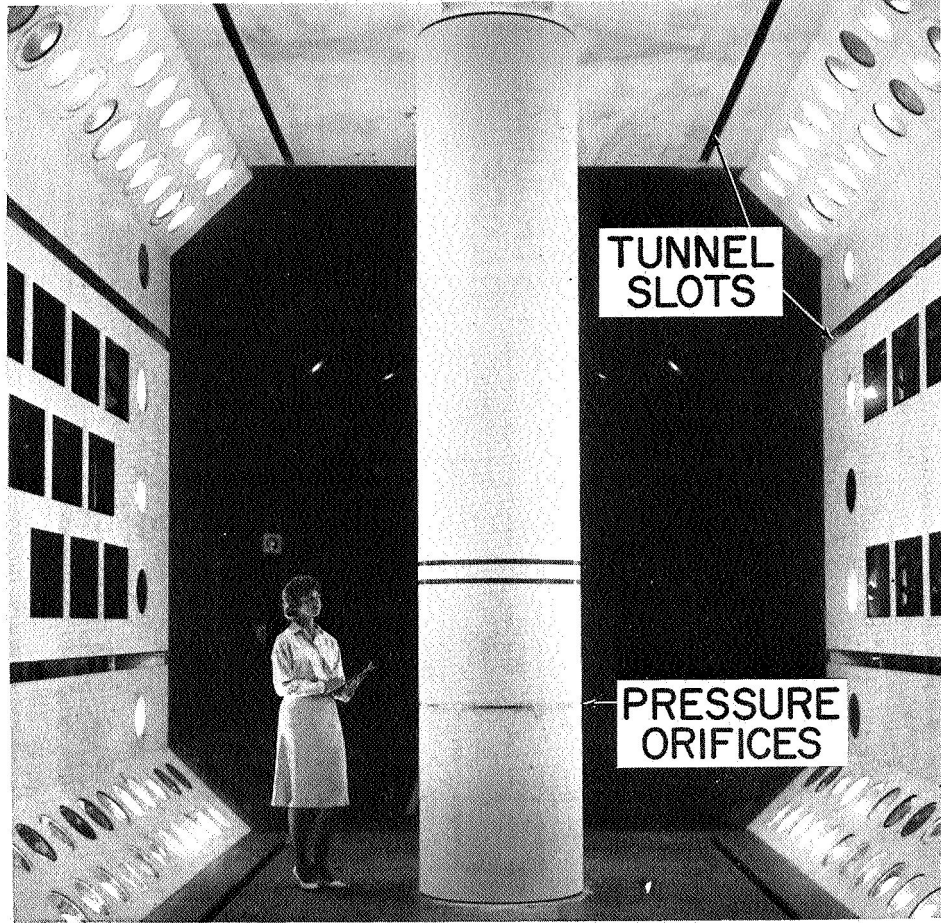


Figure 2.- Cylinder model installed in the wind tunnel.

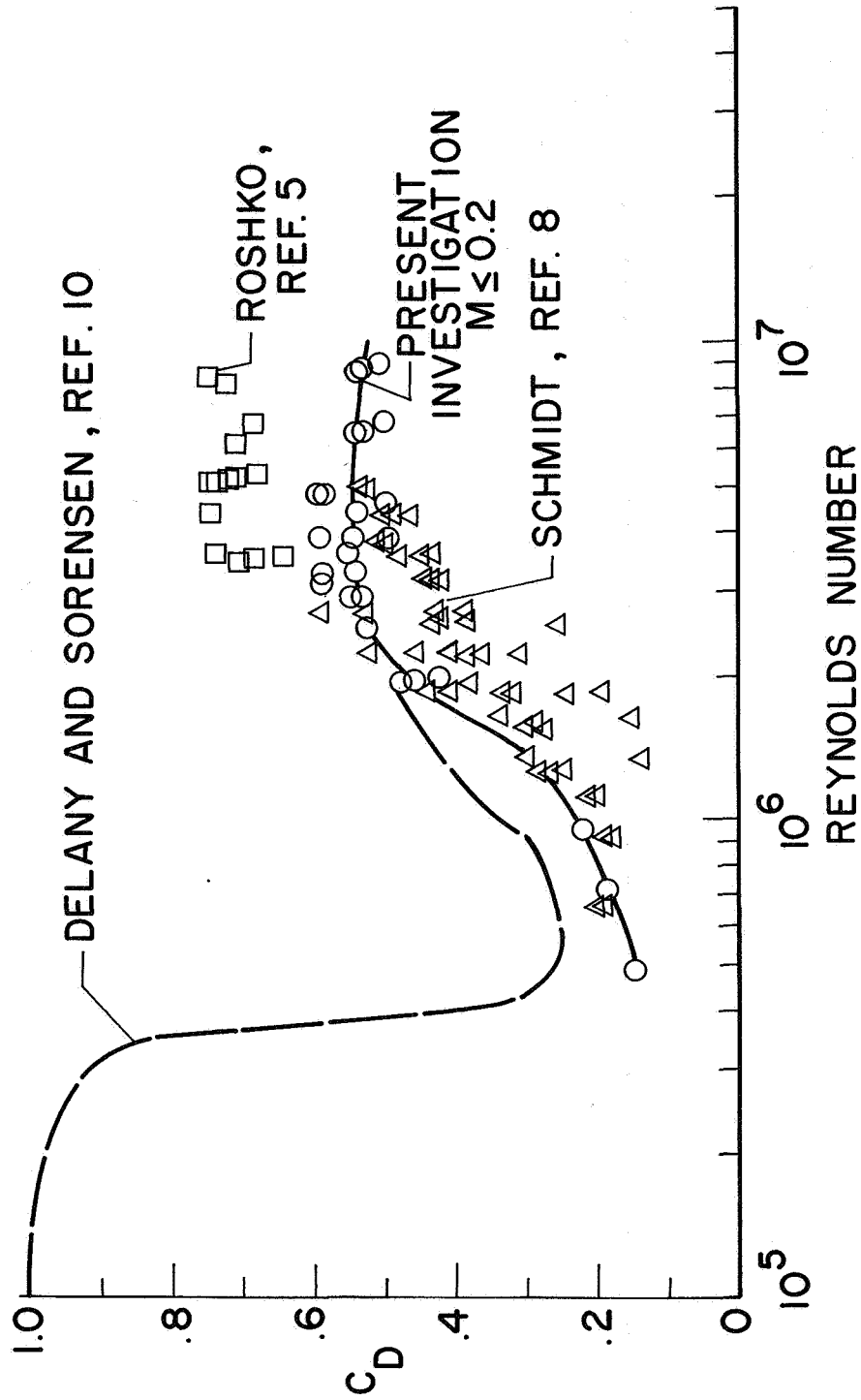


Figure 3.- Drag coefficient on stationary cylinder.

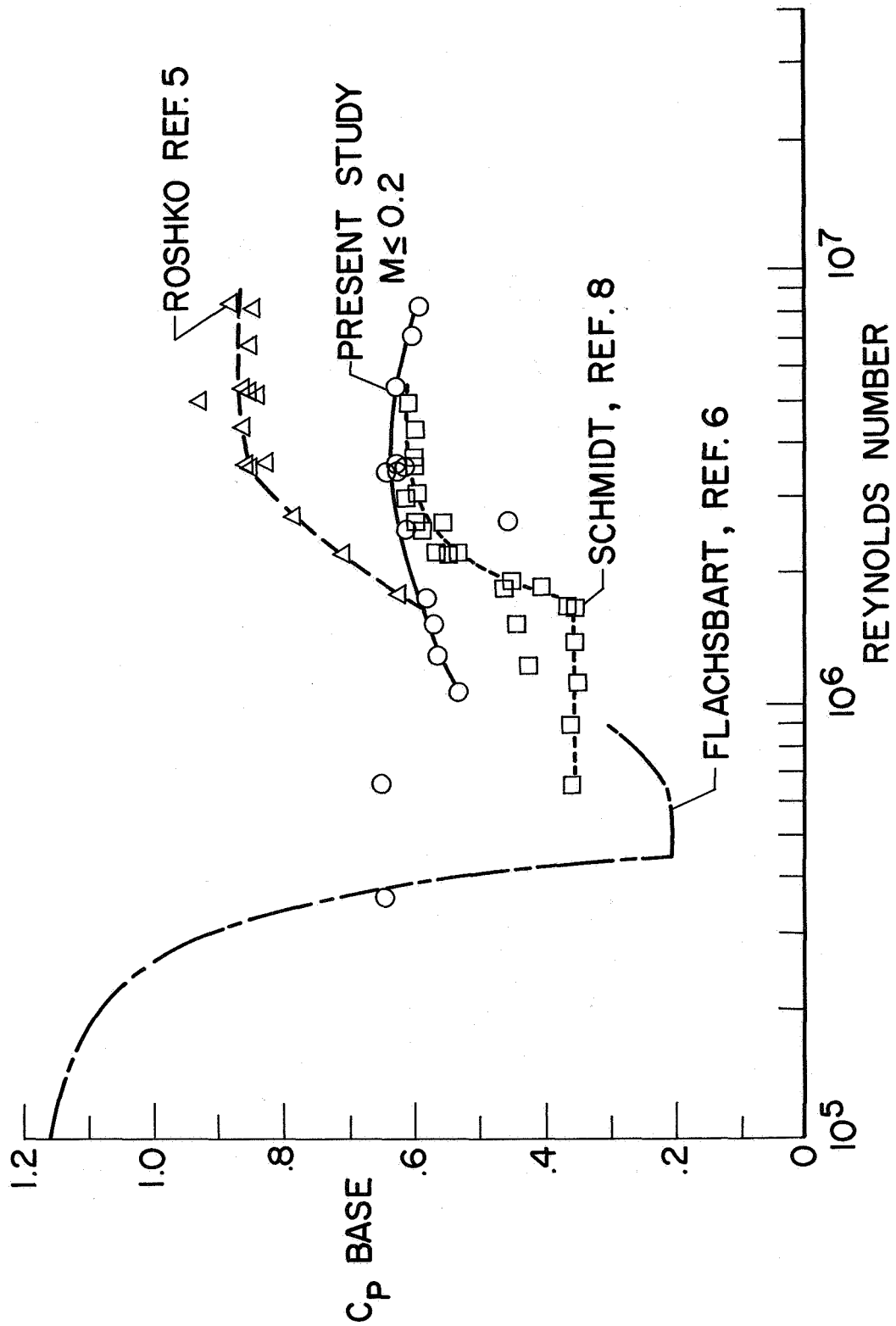


Figure 4.- Base pressure coefficient on stationary cylinder.

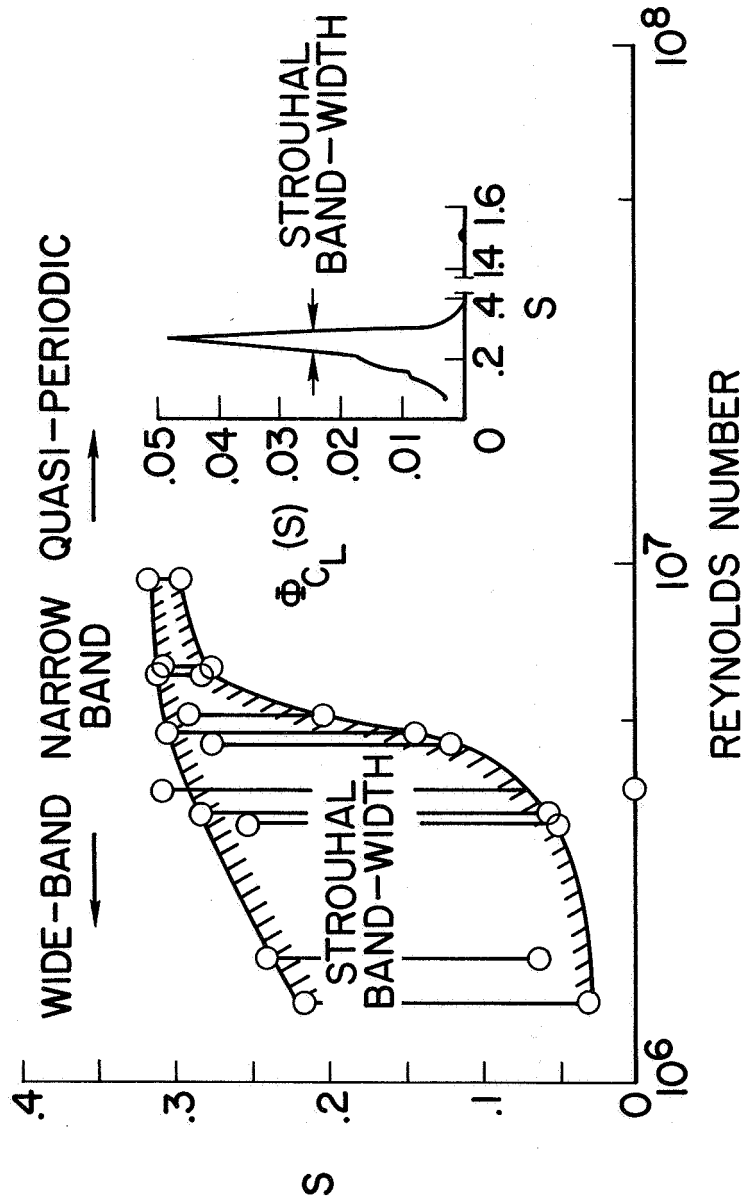


Figure 5.- Frequency content of unsteady lift on stationary cylinder.

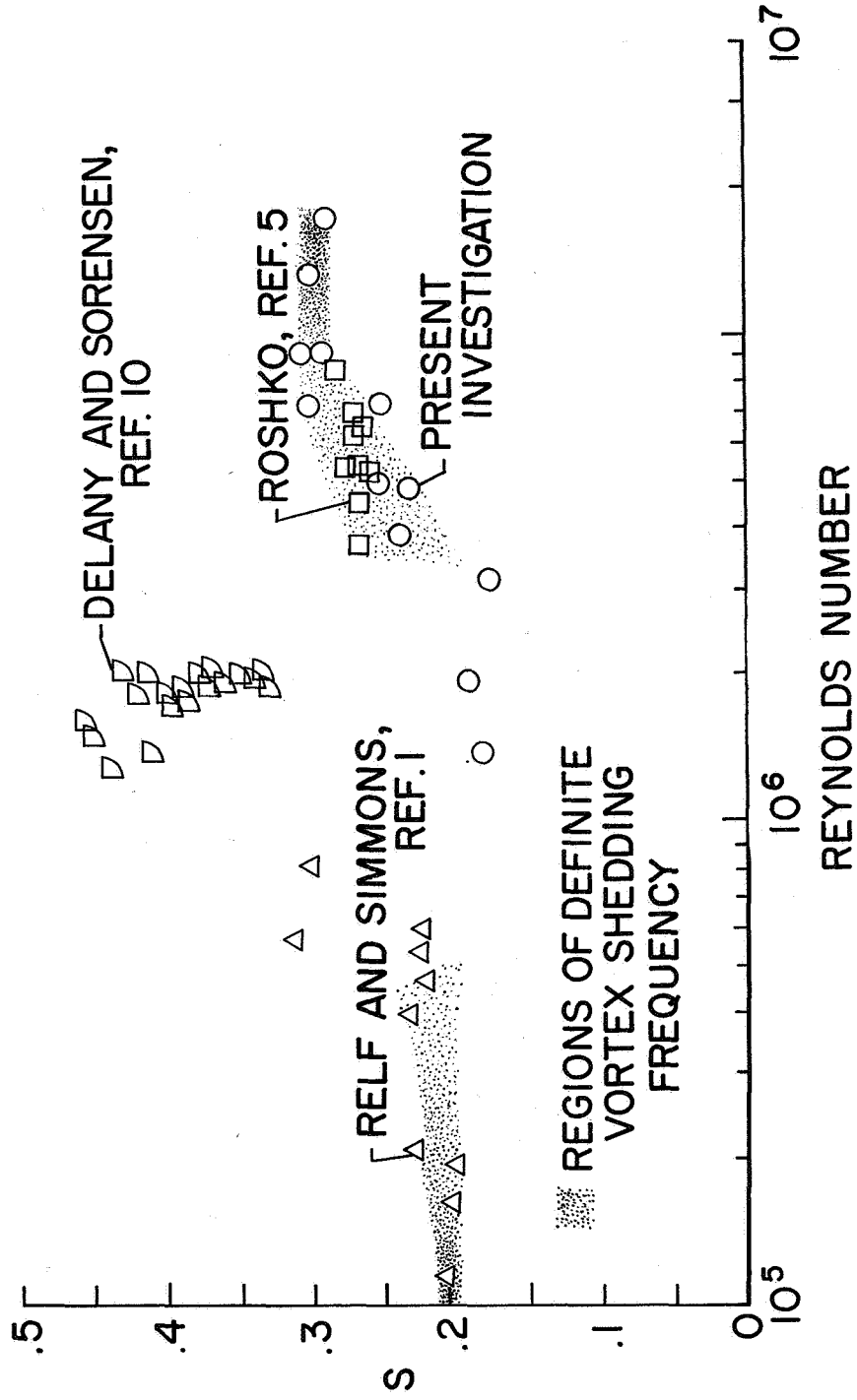


Figure 6.- Strouhal number of unsteady lift on stationary cylinder.

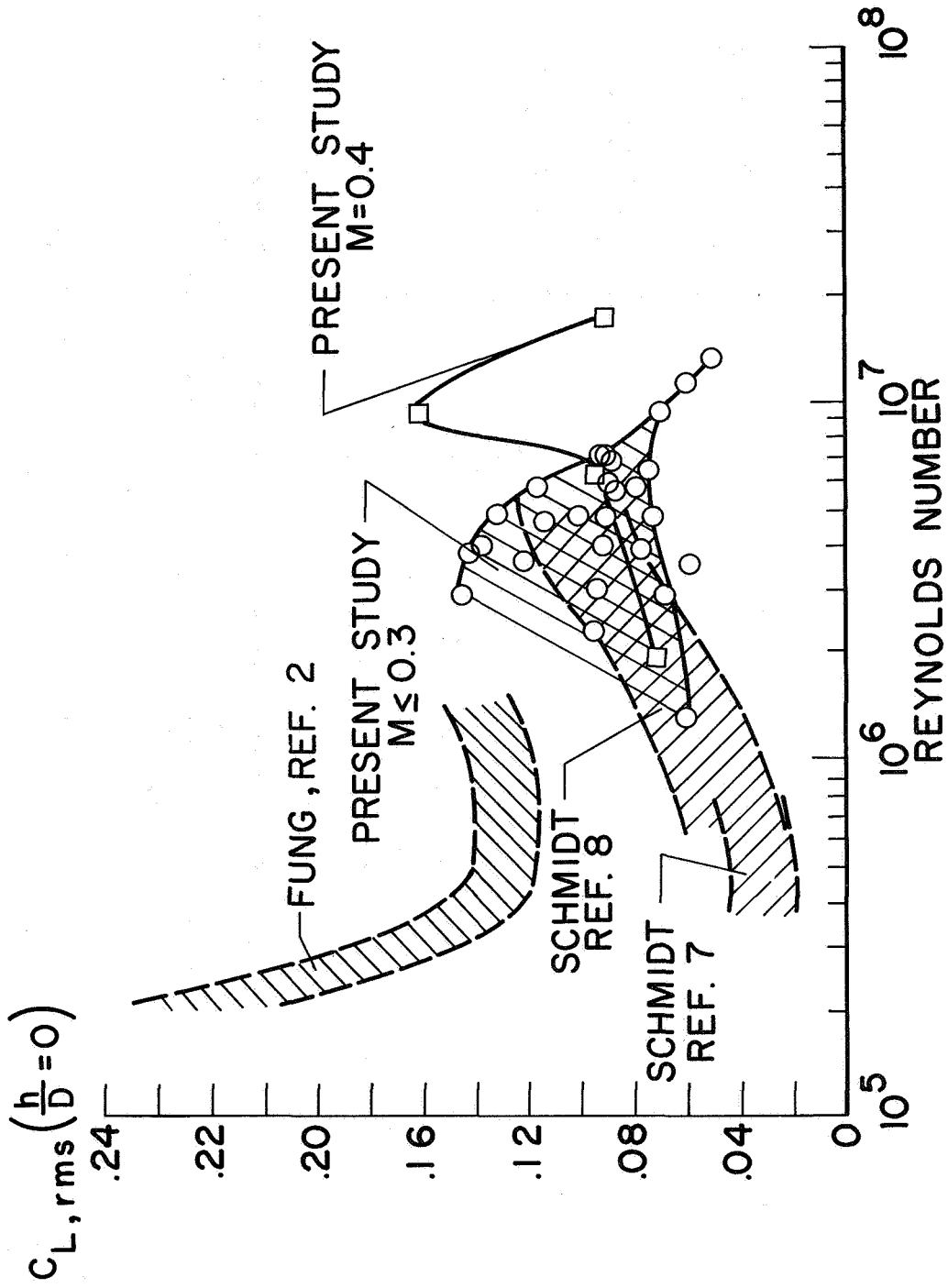


Figure 7.- Unsteady lift coefficient on stationary cylinder.

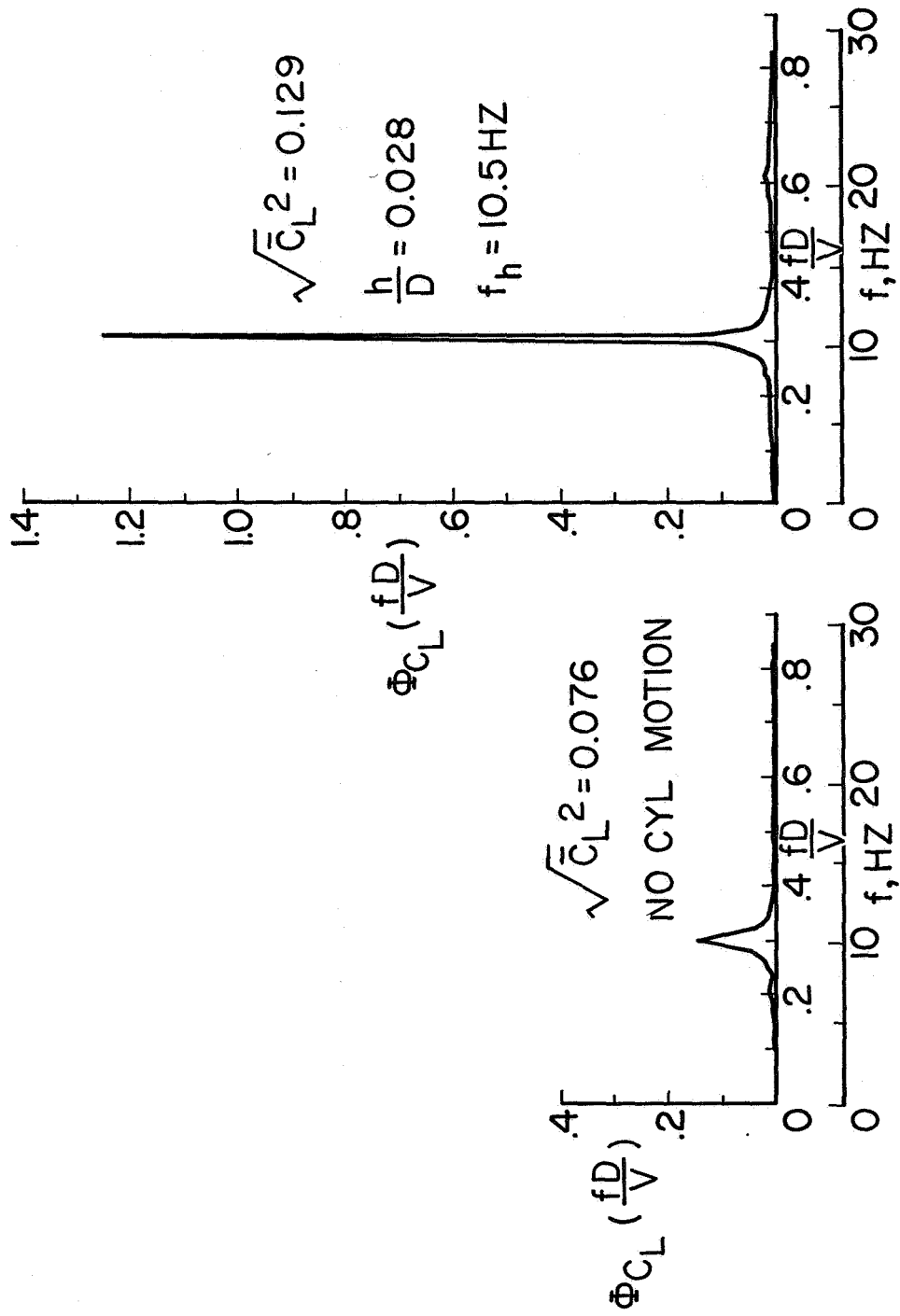


Figure 8.- PSD's of unsteady lift without and with cylinder motion.

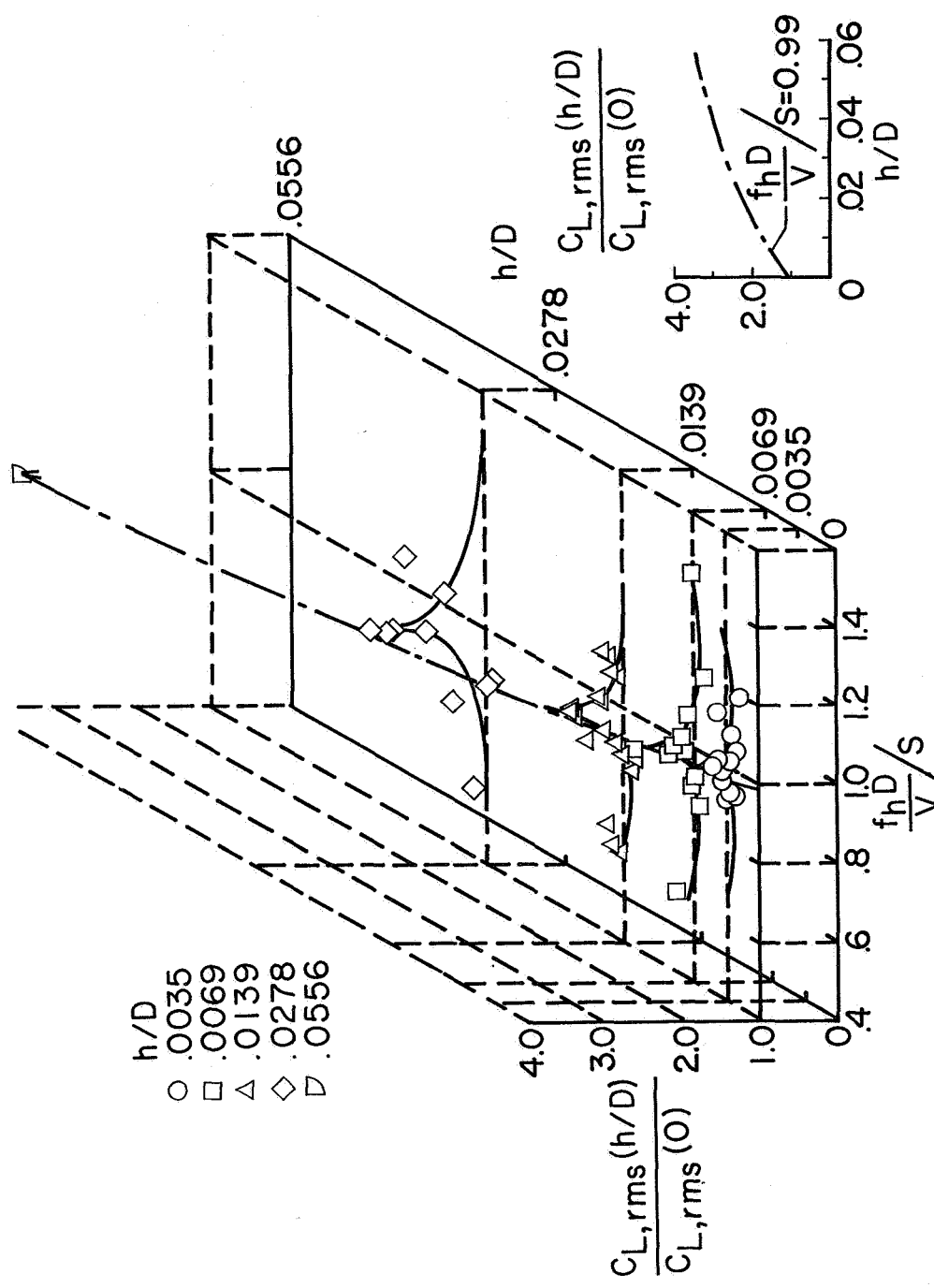


Figure 9.- Effects of cylinder motion on wide-band RMS lift coefficient.

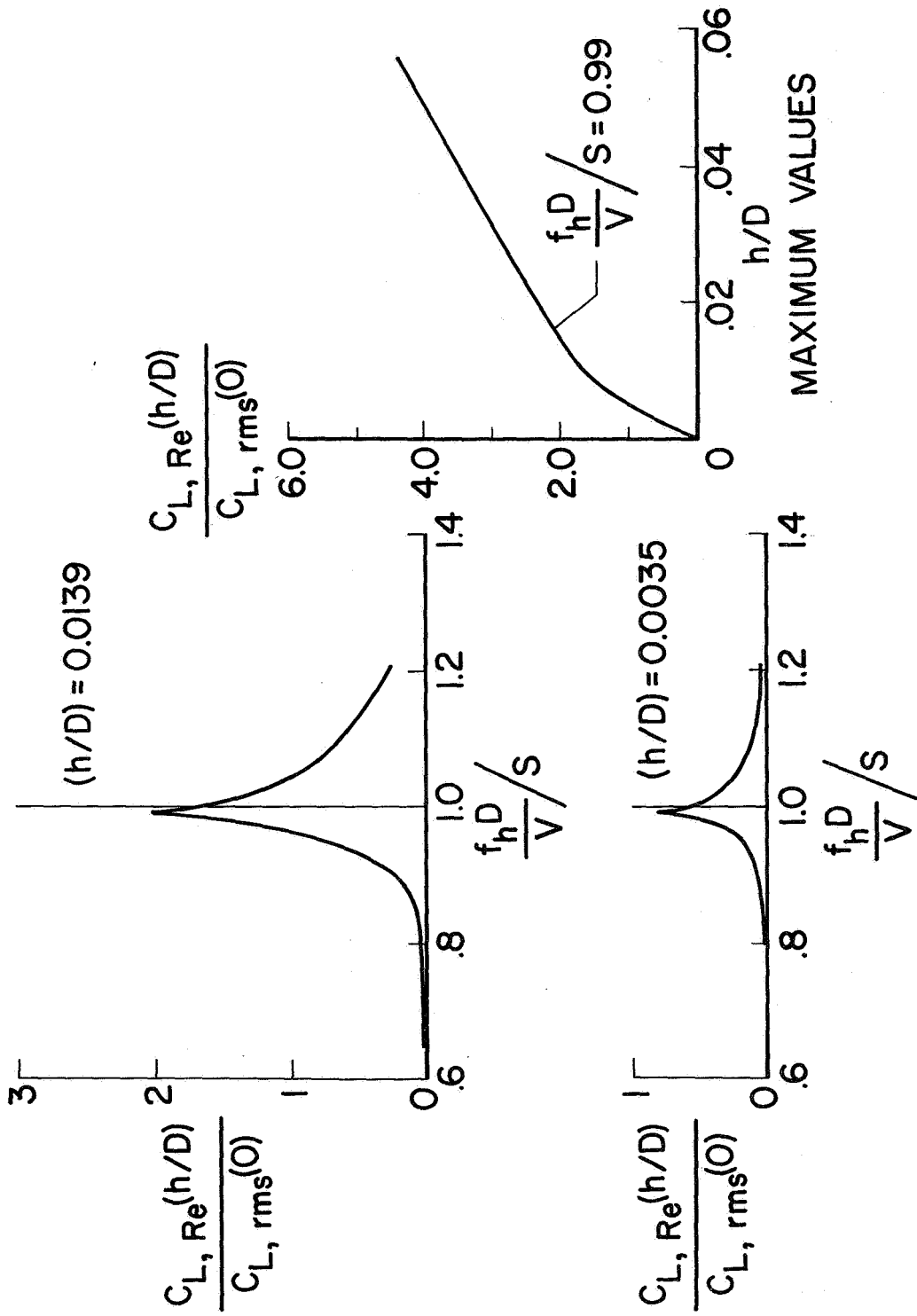


Figure 10a.- Stiffness component of unsteady lift due to cylinder motion.